Macromolecules
Cite This: Macromolecules 2019, 52, 2120−2130
Article
pubs.acs.org/Macromolecules

Impact of Nanoparticles on the Segmental and Swelling Dynamics of Ionomer Nanocomposite Membranes

Apoorv Balwani,[†] Antonio Faraone,[‡] and Eric M. Davis*[,†]

[†]Department of Chemical and Biomolecular Engineering, Clemson University, Clemson, South Carolina 29634, United States
[‡]National Institute of Standards and Technology Center for Neutron Research, Gaithersburg, Maryland 20878, United States

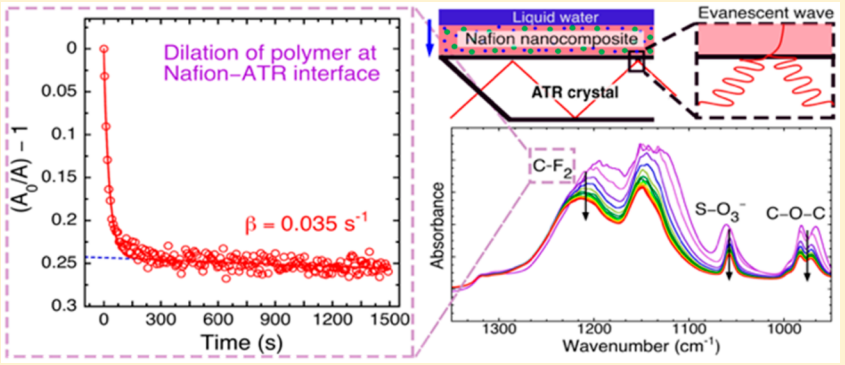

ABSTRACT: While ionomer nanocomposites show promise for advancing the viability of energy storage technologies, such as the vanadium redox flow battery, the improvements in ion selectivity are appreciable only insofar as demonstrating feasibility of these hybrid materials and are largely insufficient for wide-scale implementation of such technologies. This is in part due to our lack of understanding of how the introduction of nanoparticles (NPs) alters the morphology and dynamics of the resultant ionomer nanocomposite. Herein, we employ time-resolved attenuated total reflectance−Fourier transform infrared (*t*ATR-FTIR) spectroscopy, as well as neutron spin echo (NSE) spectroscopy, to capture the viscoelastic creep/swelling kinetics and segmental dynamics, respectively, of these ionomer nanocomposite membranes under hydration. The polymer swelling data from *t*ATR-FTIR spectroscopy experiments was fit to a three-element model to quantify the relaxation time constant for each nanocomposite at various NP loadings. In addition, NSE spectroscopy experiments on hydrated ionomer nanocomposites showed, in general, a stiffening of the segmental dynamics with increasing NP loading as well as thermal history. In addition, data from these experiments, in conjunction with previous morphological and thermomechanical studies on Nafion−SiNP nanocomposites, suggest that the NPs reside at the interface of the hydrophobic and hydrophilic phases of the ionomer, thereby altering the vanadium ion transport via slowdown of fluorocarbon chain dynamics. Results from this study have profound implications for controlling ion selectivity in these ionomer nanocomposite membranes.

INTRODUCTION

Ionomer nanocomposites prepared with silica (SiO_2) nanoparticles (SiNPs) have garnered considerable attention in recent years for effectively suppressing undesirable vanadium ion crossover in vanadium redox flow batteries (VRFBs) without significantly altering desirable proton flux through the membrane.[1−4] The most widely used ionomer material for VRFBs is Nafion, a perfluorosulfonic acid polymer wherein sulfonic acid-terminated perfluorovinyl ether chains are grafted onto a Teflon-like backbone. In hydrated environments, the ionomer exists in a nanophase-segregated morphology, where the hydrophilic sulfonic groups form ionic channels that facilitate transport of protons and ions, while the hydrophobic Teflon-like domain provides excellent chemical and mechanical stability.[1,5,6] Nafion nanocomposites have been exhaustively investigated for their excellent methanol crossover resistances in direct methanol fuel cells (DMFCs),[7−12] motivating their implementation in VRFBs to combat the poor ion selectivity of the unmodified membrane. These ionomer nanocomposites have traditionally been fabricated using an *in situ* sol−gel condensation process,[1−3,7] whereby a preformed Nafion membrane is imbibed with precursor silica sol that, under heat, reacts to form a "condensed" silica phase within the membrane. More recently, these composites have been fabricated via solution-casting, as this technique provides the ability to introduce discrete nanoparticles of prescribed size and surface chemistry into the ionomer membrane.[11,13] In contrast to sol−gel nanocomposites, solution-cast membranes are fabricated by casting a dispersion (solution) of Nafion and SiNPs and allowing the solvent to evaporate, thereby forming a dense, nanocomposite membrane.

Received: October 11, 2018
Revised: December 27, 2018
Published: February 20, 2019

DOI: 10.1021/acs.macromol.8b02189
Macromolecules 2019, 52, 2120−2130

In Nafion−SiO_2 nanocomposites, the nanoparticles are traditionally understood to be preferentially sequestered into the ionic channels, where they impede movement of hydrated vanadium ions via a size exclusion mechanism.[3,14] In addition, Schwenzer et al.[7] suggested that interactions between the sulfonic groups in the ionic channels and the SiNPs could render many sulfonic groups inaccessible for vanadium ion diffusion. However, a significant number of reports observe modifications to the thermomechanical behavior (e.g., α- and β-relaxations) of Nafion when SiNPs are introduced into the unmodified ionomer matrix.[15−18] This is reminiscent of similar effects reported in other nanoparticle-modified systems[19−24] and indicates that interfacial interactions between the polymer chains and nanoparticles are more enhanced than if the nanoparticles resided primarily in the ionic channels of the ionomer.[17,25,26] As such, these interactions may not be entirely dependent on the sulfonic activity in the ionic channels.[12,27−30]

Previous studies using wide-angle X-ray spectroscopy have also reported perturbations at length scales correlating to the chain packing in the hydrophobic phase due to presence of SiNPs.[12,31,32] In addition, small-angle neutron scattering (SANS) experiments on Nafion−SiO_2 reported by Davis and co-workers[1] suggest that nanoparticles are too big to solely reside within the ionic channels and are predominantly present in the hydrophobic bulk. This was verified by the presence of large SiNP aggregates (hundreds of nanometers in diameter) in the transmission electron microscopy (TEM) images. The authors also found that annealing neat Nafion ionomer membranes was as effective in reducing vanadium ion crossover as the introduction of SiNPs. These results present an interesting conundrum, as the SiNPs may not be directly interacting with vanadium ions as has previously been thought (i.e., by steric impedance). Rather, transport through the ionic channels in Nafion may be coupled to the polymer chain (segmental) dynamics and morphology.[33−35]

Recent studies indicate that the Nafion morphology and segmental dynamics are affected at the Nafion−nanoparticle interface,[36−39] where morphological variations at the interface were found to be specific to the nature of nanoparticle surface (hydrophobic vs hydrophilic), which engendered different nanophase ordering within Nafion in each case. Separately, a vast body of work highlights the impact of nanoparticles on the segmental dynamics and consequently glass transition temperatures in noncharged systems (e.g., SiNPs in a poly(methyl methacrylate) matrix).[21,22,40−44] Thus, it is an ongoing challenge to correlate how the altered morphology in the "bound" Nafion layer (i.e., Nafion−SiO_2 interface) results in bulk-scale dynamics of the ionomer nanocomposite system.

To probe the effect of nanoparticles on the segmental dynamics and viscoelastic behavior of Nafion, two series of nanocomposite membranes were prepared using extruded Nafion 117 films (sol−gel series) and Nafion 1100 resin solution (solution-cast series). At least two of the membranes in each series contained SiO_2 at a loading of approximately 4% (by mass) and 10% (by mass). Note that here that "% (by mass)" denotes mass of SiO_2 per mass of Nafion solids (i.e., g SiO_2/g Nafion). All nanocomposite samples prepared via the sol−gel method were subjected to thermal treatment (140 °C for 2 h) as part of the synthesis process. The thermal treatment, herein also termed "annealing", is performed at a temperature well above the glass transition temperature of the Nafion ionomer and is expected to enhance the degree of order in the fluorocarbon chain packing within the membrane.[45] Thus, to investigate the impact of crystallinity on the sorption kinetics and polymer dynamics, these nanocomposite membranes were compared to unmodified Nafion membranes (no SiNPs), which were either unannealed (no heat treatment) or annealed (140 °C for 2 h).

In this study, we investigate nanoscale segmental relaxation dynamics and bulk swelling kinetics of Nafion−SiO_2 nanocomposites prepared by both sol−gel and solution-casting methods. Specifically, the diffusion-induced polymer swelling dynamics are characterized using time-resolved attenuated total reflectance−Fourier transform infrared (*t*ATR-FTIR) spectroscopy. The swelling data were fit to a three-element viscoelastic model[46] to gain insight into how the creep response of Nafion under osmotic stress is altered by the presence of SiNPs. In addition, the segmental dynamics of the Nafion−SiO_2 membranes were probed via neutron spin echo (NSE) spectroscopy.[47] To the best of our knowledge, this is the first time the molecular-level polymer dynamics in solution-cast and sol−gel synthesized Nafion−SiO_2 membranes have been reported.

MATERIALS AND METHODS

Materials. Nafion perfluorinated resin solution (20% (by mass) in mixture of lower aliphatic alcohols and water, equivalent weight = 1100 g/mol sulfonic acid), tetraethyl orthosilicate (TEOS, >99.0% purity), methanol (HPLC grade, ≥99.9% purity), sulfuric acid (95%−98% purity, ACS reagent), and deuterium oxide (D_2O, 99.9 atom % D) were purchased from Sigma-Aldrich. Silicon oxide nanoparticles (99.5% purity, 10−20 nm particle size, nonporous) were obtained from Nissan Chemicals as a dispersion in methanol (30% (by mass) silica). Extruded Nafion 117 membranes (thickness ≈ 180 μm, equivalent weight = 1100 g/mol sulfonic acid) were obtained from Ion Power Inc. Hydrogen peroxide (30% (by mass) in H_2O) was procured from VWR International. Additionally, reverse osmosis (RO) water (resistivity ≈ 18 MΩ·cm) and dry nitrogen gas were used for all liquid water polymer swelling experiments.

Membrane Purification. Prior to use, commercially procured Nafion 117 membranes were purified and protonated. Specifically, the membranes were cut into 4 cm × 9 cm strips (for NSE spectroscopy experiments) or to the size of the ATR crystals (for *t*ATR-FTIR spectroscopy experiments) and refluxed for 1 h in 3% (by mass) hydrogen peroxide, followed by deionized water, then 0.5 mol/L sulfuric acid, and finally deionized water. After each step, the membranes were thoroughly washed with deionized water. Finally, the purified films were dried at 90 °C under vacuum for 24 h to obtain dry polymer mass. Note that when nanocomposite films were prepared via solution casting, this purification step was not employed.

Preparation of Nafion−SiO_2 Nanocomposite Membranes via the Sol−Gel Method. After purification, dried Nafion 117 strips were equilibrated in a 2:1 (v/v) methanol/water solution for 4 h at room temperature. Following equilibration, a solution of TEOS and methanol (TEOS:methanol = 1.5:1 (v/v)) was added to a stoppered flask containing the equilibrated films as well as 50 mL of the methanol/water solution in which the films were equilibrated. The quantity of TEOS−methanol solution introduced in the flask was determined as to maintain the water to TEOS molar ratio at 4:1. Immediately after addition of TEOS, the flasks were sealed for the desired residence times (i.e., the time the film was left to soak in the precursor solution). Once removed from the reaction flasks, the films were washed with pure methanol and blotted dry to prevent gelation on the surface.

Next, the films were dried at room temperature for 24 h, followed by thermal treatment (annealing) for 2 h at 140 °C, after which the oven was allowed to cool to room temperature. The entire process (from drying to annealing to cooling) was performed under dynamic vacuum. To prevent delamination issues during *t*ATR-FTIR characterization (i.e., membrane not being properly adhered to the

DOI: 10.1021/acs.macromol.8b02189
Macromolecules 2019, 52, 2120−2130

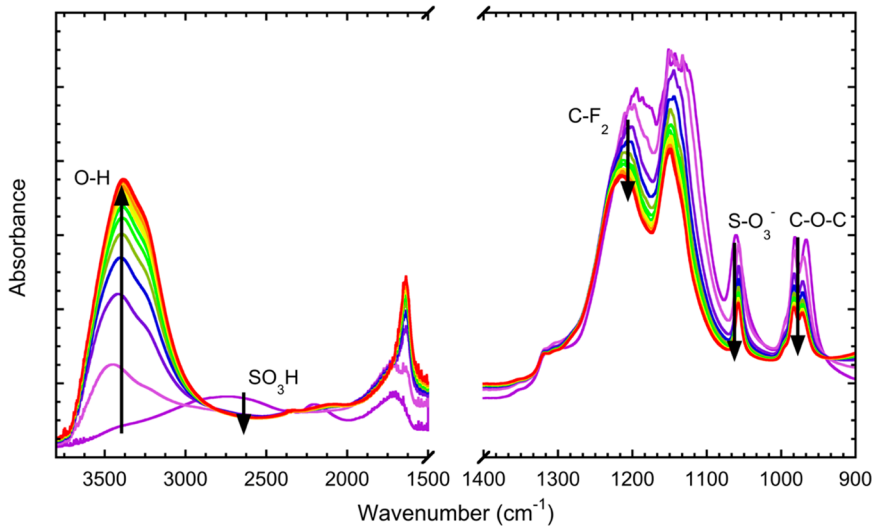

Figure 1. Infrared spectra of liquid water diffusing into dry, unannealed, unmodified Nafion at 25 °C at selected time intervals. Arrows indicate the direction of spectral change with time.

ATR crystal), samples prepared for these experiments were clamped between two 105 mm × 15 mm Teflon plates prior to being placed in the vacuum oven. Finally, the dry, annealed Nafion−SiO_2 nanocomposite films were weighed to obtain the mass of silica phase in the films.

Preparation of Nafion−SiO_2 Nanocomposite Membranes via the Solution-Cast Method. A series of Nafion−SiO_2 dispersions were prepared (with silica content ranging from 0% (by mass) to 10% (by mass)) by transferring "as-received" Nafion stock solution into a 25 mL scintillation vial and adding the appropriate amount of silica nanoparticles. The vials were sonicated for 3−4 h to ensure uniform dispersion. The suspensions were then cast into a 5 cm × 7.5 cm polydimethylsiloxane mold, which was placed in a Teflon Petri dish (for samples for NSE experiments) or onto a trapezoidal, multireflection germanium crystal (for *t*ATR-FTIR experiments) and allowed to dry at room temperature overnight. Membranes prepared via solution casting had thicknesses of ≈150 μm. For membranes requiring thermal treatment, the polymer-coated crystals were placed under dynamic vacuum and heated to 140 °C for 2 h, followed by cooling to room temperature, before removing the films. For NSE samples requiring thermal treatment, the samples were carefully peeled from the Teflon dish using a pair of tweezers prior to the aforementioned annealing step.

Time-Resolved ATR-FTIR Spectroscopy. For liquid water ionomer swelling measurements, time-resolved infrared spectra were collected using a Fourier transform infrared (FTIR) spectrometer (Nicolet iS50R FT-IR spectrometer; Thermo Scientific), which was equipped with horizontal, temperature-controlled attenuated total reflectance (ATR) cell (Gateway ATR accessory; Specac, Inc.). For solution-cast membranes, the polymer films were deposited on a multiple reflection, trapezoidal germanium (Ge) ATR crystal (Specac, Inc., 45° beveled faces). For extruded Nafion 117 membranes, the preformed membranes were "physisorbed" onto the surface of a zinc selenide (ZnSe) ATR crystal (Specac, Inc.) as previously described.[48] All infrared spectra were collected using a liquid nitrogen cooled mercury−cadmium−telluride detector at a rate of two scans per spectrum and a resolution of 4 cm^{-1}, resulting in a repeat collection time of ≈0.78 s for *t*ATR-FTIR experiments.

Prior to liquid water swelling experiments, a background spectrum of the ATR crystal was collected, and all subsequent spectra were subtracted from this spectrum. Next, a polymer-coated ATR crystal (either Ge or ZnSe) was mounted into the flow-through ATR cell by placing a Kalrez gasket between the top plate and the top side of the film. Then the cell was sealed. Once the flow through cells were mounted on the ATR accessory, the films were dried in high-purity nitrogen for ∼4 h before beginning each experiment.

To begin liquid water swelling experiments, reverse osmosis water was pipetted into the ATR cell in the space above the polymer film (V = 550 μL; the side opposite the polymer−crystal interface) and sealed to prevent water evaporation during experiments. This was followed by time-resolved infrared spectral collection. All spectra were collected at 25 °C, which was controlled by a temperature bath. Immediately following each experiment, the thickness of the hydrated membranes was measured using a digital micrometer (Mitutoyo) with a 1 μm accuracy. Each film thickness was an average of five individual measurements at different positions along the length of the film.

Neutron Spin Echo Spectroscopy. NSE experiments were performed on the NGA neutron guide at the National Institute of Standards and Technology Center for Neutron Research (NCNR) to characterize the dynamics within Nafion−SiO_2 nanocomposites at a scattering vector (Q) = 1.2 and 1.3 $Å^{-1}$, which correlate to the lateral packing length scale of the polymer chains. The neutron wavelength was set to 6 Å with a $\Delta\lambda/\lambda \approx 20\%$. At this wavelength, a time range of 5 ps−15 ns was available.

Prior to running the experiments, resolution and background scattering data were collected using a titanium−zirconium alloy sample and an aluminum empty cell, respectively. Next, the membranes were equilibrated in D_2O overnight to minimize the incoherent scattering from hydrogen. Once equilibrated, the membranes were cut into the appropriate dimensions and sandwiched between aluminum foil before being sealed inside aluminum cells. To ensure good collection statistics, multiple membranes were "stacked" inside of the aluminum cell to obtain an overall thickness of ≈1 mm (anywhere from 5 to 7 membranes). Note that all samples prepared via solution-casting were annealed before characterizing them using NSE spectroscopy, as unannealed samples were prone to tearing and dissolution when hydrated.

At the start of each experiment, polarized diffraction measurements were made at a Fourier time of 0.5 ns in the Q range of 0.1−1.5 $Å^{-1}$ to obtain a quantity proportional to $S(Q,0)$ and the ratio between coherent and incoherent scattering. For each experiment, the data were normalized to the intermediate structure factor at time t = 0 (i.e., $S(Q,t)/S(Q,0)$), after normalization of all data sets for the instrumental energy resolution. All measurements were made at 298 K. The raw data sets were reduced and fit using DAVE, an in-house data analysis and visualization software employed at NIST which consists of macros for data reduction and analysis.[49]

RESULTS AND DISCUSSION

Swelling/Reorganizational Dynamics of Ionomer Nanocomposites. Figure 1 shows the time-resolved infrared

DOI: 10.1021/acs.macromol.8b02189
Macromolecules 2019, 52, 2120−2130

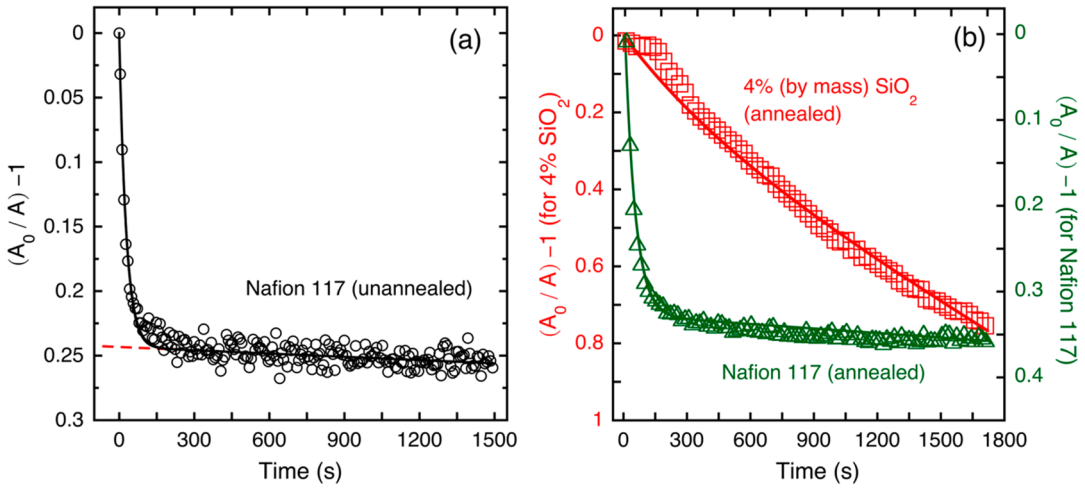

Figure 2. Time-resolved absorbance data of the polymer backbone CF_2 stretching as a function of time at 25 °C for extruded (a) unannealed Nafion 117 and (b) annealed Nafion 117 with no silica (open green triangles) and with 4% (by mass) silica (open red squares), The solid lines represent the full solution of eq 1, where the relaxation time constant (β) was the only adjustable fitting parameter. The thermal treatment conditions of all the samples are indicated (in parentheses) next to the sample name.

spectra of liquid water diffusing into unannealed, unmodified Nafion at 25 °C at the polymer−ATR crystal interface, where time t = 0 represents when the water was injected into the ATR flow-through cell. It can be seen that the intensity of the infrared band associated with the O−H stretching of water (peak centered at ≈3400 cm^{-1}) increases with time, while the intensity of the infrared band associated with the F−C−F stretching of Nafion (peak centered at ≈1200 cm^{-1})[46,50] decreases with time. The increase in O−H stretching is attributed to the diffusion of water through the thickness of the film, and the decrease in F−C−F stretching is representative of water-induced relaxation of the polymer.

The diffusion-relaxation behavior shown by the time-resolved spectra in Figure 1 has been previously observed for water diffusion in Nafion membranes. In particular, Hallinan and co-workers[46,51] observed anomalous, non-Fickian diffusion of water vapor in Nafion 117 when the Nafion was exposed to relative humidity (RH) jumps from 0% RH to 100% RH. They attributed the non-Fickian behavior to osmotic stress dissipation (i.e., water-induced viscoelastic relaxation), leading them to propose a three-element viscoelastic relaxation model to describe the coupling of water sorption kinetics and swelling of ionic domains due to diffusing water molecules. The applied stress (σ_0) and the strain (ε) can be related to the F−C−F infrared absorbance of Nafion with time ($A(t)$) through the equation

$$\varepsilon \approx \frac{A_0}{A(t)} - 1 = \frac{\sigma_0}{\eta}t + \frac{\sigma_0}{E}(1 - \exp(-\beta t)) \quad (1)$$

where A_0 is the absorbance of the F−C−F infrared band at time t = 0, η is the viscosity of the hydrophobic region, E is the elastic modulus, and β is the creep relaxation (or swelling) time constant. That is, the dilution of the F−C−F infrared band with time due to molecular rearrangement/swelling of the hydrophilic ionic network can be analyzed with the above diffusion-driven polymer creep relaxation equation to obtain a viscoelastic time scale for water-induced swelling in the membrane. More information regarding the model can be found elsewhere.[46,52]

Figure 2a shows the "factorized" (to their initial, unstrained-state value), initialized integrated absorbance of the F−C−F infrared band (A_0/A − 1) as a function of time for an unmodified, unannealed (i.e., no SiNPs and no thermal treatment) Nafion 117 membrane. Per eq 1, the integrated absorbance represents the volumetric strain within the Nafion−SiO_2 nanocomposite films due to stresses imposed by diffusing water. The dotted red line in Figure 2a is the best-fit regression of the late-time ionomer relaxation data to the late-time solution of eq 1 (as $t \rightarrow \infty$), where the slope (σ_0/η) is 8.46 × 10^{-6} ± 1.11 × 10^{-6} s^{-1} and the y-intercept (σ_0/E) is 0.243 ± 0.001 (R^2 = 0.91). With these parameters now determined, the full set of relaxation data for the unmodified, unannealed Nafion 117 membrane can be fit to eq 1, with the relaxation time constant, β, as the only adjustable parameter. From this analysis, a relaxation time constant of β = 0.035 ± 0.000 s^{-1} (R^2 = 0.91) was obtained. It should be noted that the polymer relaxation dynamics observed herein are at a much faster time scale than those previously observed by water vapor diffusion experiments. Consequently, viscoelastic relaxation constants obtained in this study were 1−2 orders of magnitude higher than those previously reported,[46] indicating that significantly larger stresses are developed in the presence of liquid water than if 100% RH water vapor is sorbed.

This analysis was extended to sol−gel synthesized Nafion−SiO_2 nanocomposite membranes (Figure 2b). From Figure 2b, we see that both the annealed and 4% (by mass) Nafion membranes exhibit slowed down swelling (relaxation) dynamics as compared to the unannealed, unmodified Nafion membrane (Figure 2a). Specifically, the relaxation time constants were determined to be β = 0.024 ± 0.000 s^{-1} and β = 0.002 ± 0.001 s^{-1} (R^2 = 0.99 in each case) for the unmodified, annealed Nafion membrane (open green triangles) and Nafion containing 4% (by mass) SiO_2 (open red squares), respectively. A summary of the relaxation model analysis for Nafion 117 and sol−gel membranes is presented in Table 1. Note that the values listed in the table are an average of multiple (at least three) experiments, and the ± values represent the standard deviation of the calculated, averaged parameter.

As we can see from Table 1, both annealing the Nafion 117 and the introduction of an SiO_2 phase via sol−gel condensation in the membranes significantly alter the

DOI: 10.1021/acs.macromol.8b02189
Macromolecules 2019, 52, 2120−2130

Table 1. Normalized Relaxation Time Constant for Nafion and Nafion Nanocomposite Membranes Prepared by Both Sol−Gel and Solution-Cast Methods[a]

membrane	normalized relaxation time constant [β_{norm}] (10^{-6} cm^2/s)
sol−gel membranes	
Nafion 117 (unannealed)	11.1 ± 2.0
Nafion 117 (annealed)	5.8 ± 1.7
Nafion/SiO_2 nanocomposite, 4% (by mass) SiO_2 (annealed)	0.8 ± 0.2
Nafion/SiO_2 nanocomposite, 10% (by mass) SiO_2 (annealed)	3.0 ± 1.3
solution-cast membranes	
Nafion (unannealed)	4.6 ± 1.1
Nafion (annealed)	15.3 ± 2.8
Nafion−SiO_2 nanocomposite, 4% (by mass) SiO_2 (unannealed)	7.9 ± 1.1
Nafion−SiO_2 nanocomposite, 4% (by mass) SiO_2 (annealed)	6.2 ± 3.0
Nafion−SiO_2 nanocomposite, 10% (by mass) SiO_2 (annealed)	4.6 ± 1.6

[a]The thermal treatment conditions of all the samples are indicated (in parentheses) next to the sample name. Note that the values listed in the table are an average of multiple (at least three) experiments, and the ± values represent the standard deviation of the calculated, averaged parameter. Note that instead of presenting the relaxation time constant, β, we have "normalized" (scaled with the square of the thickness of the membrane) the calculated time constant. For *t*ATR-FTIR experiments, relaxation (or swelling) of the membrane only occurs due to the diffusion of water into the membrane. As the time scale for diffusion for each experiment is a function of the membrane thickness, we must normalize the water-induced relaxation time constant to accurately compare relaxation data obtained for membranes with different thicknesses (i.e., $\beta_{norm} = L^2 \times \beta$, where L is the thickness of the membrane). Treatment of the FTIR swelling data in this manner has previously been reported for this experimental technique.[53,54]

swelling/rearrangement dynamics of the extruded Nafion 117 membrane. By heat-treating the Nafion 117 membrane, we observe an ≈50% reduction in the "normalized" relaxation time constant, implying that the ionomer network has become stiffer. This increase in membrane stiffness can be attributed to an increase in crystallinity and modulus of the membrane, both of which have been shown to increase with annealing.[1] We observe an additional 7-fold decrease in the viscoelastic relaxation dynamics of the annealed Nafion 117 membrane with the introduction of 4% (by mass) SiO_2. Furthermore, the β_{norm} value for the 4% (by mass) SiO_2 membrane was over an order of magnitude smaller than that calculated for unannealed Nafion 117 membranes.

However, when the SiO_2 loading is increased from 4% (by mass) SiO_2 to 10% (by mass) SiO_2, the value of β_{norm} increases ≈260% to a value much closer to that obtained for annealed Nafion 117 membranes. This result is quite interesting as it follows, at least qualitatively, recent work by Davis and co-workers[1] on sol−gel synthesized Nafion 117 nanocomposites. In their work, the vanadium ion crossover resistance for an ≈10% (by mass) SiO_2 membrane was determined to be moderately improved over that for annealed, unmodified Nafion membranes (9.7×10^{-9} cm^2/s vs 11.0×10^{-9} cm^2/s), while over 4 times better than that obtained for unannealed, unmodified Nafion membranes (9.7×10^{-9} cm^2/s vs 44.0×10^{-9} cm^2/s).

As seen in Table 1, the calculated values of β_{norm} show an analogous trend of decreasing relaxation dynamics, where the swelling dynamics show unannealed > annealed > 10% (by mass) SiO_2. Unfortunately, the previously mentioned study did not perform permeation studies on Nafion 117 membranes containing 4% (by mass) SiO_2, so it is unknown at this time how the significantly reduced swelling dynamics of these membranes translate to permeability of vanadium ions. In any case, current results from *t*FTIR-ATR spectroscopy experiments, when taken in conjunction with each other, begin to allude to a scenario where alterations in the Nafion membrane dynamics may play a significant role in controlling the ion selectivity of these membranes.

In contrast to sol−gel synthesized membranes, solution-cast films were created by casting from a dispersion of Nafion and SiNPs in a mixture of low aliphatic alcohols and water, where

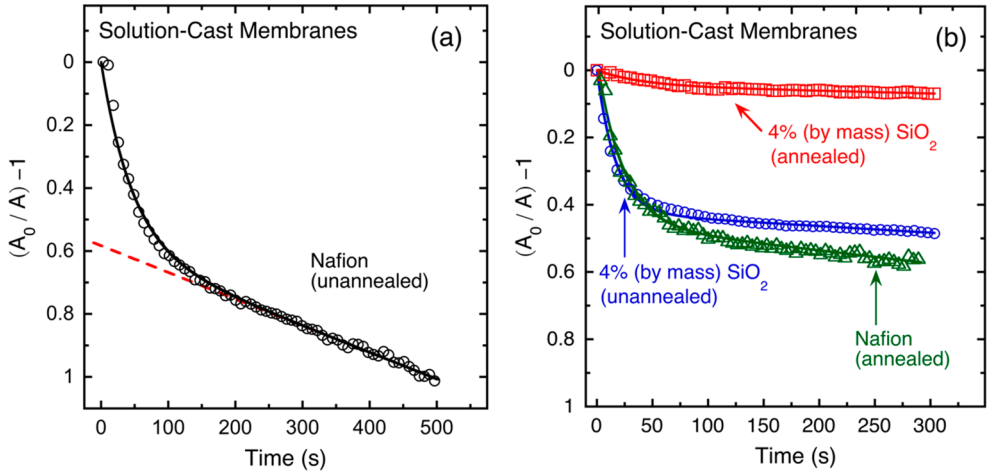

Figure 3. Time-resolved absorbance data of the polymer backbone CF_2 stretching as a function of time at 25 °C for solution-cast (a) unannealed Nafion and (b) annealed Nafion (open green triangles), unannealed 4% (by mass) silica (open blue circles), and annealed 4% (by mass) silica (open red squares). The dashed red line in (a) is the best-fit regression of the late-time absorbance data to the late-time solution of eq 1. The solid lines in both figures represent the full solution of eq 1, where the relaxation time constant (β) was the only adjustable fitting parameter. Note that only 20% of the time-resolved data are shown for clarity. The thermal treatment conditions of all the samples are indicated (in parentheses) next to the sample name.

DOI: 10.1021/acs.macromol.8b02189
Macromolecules 2019, 52, 2120−2130

the final dense membrane was formed after solvent evaporation. Figure 3a illustrates the diffusion-driven polymer relaxation in solution-cast membranes, described herein as factorized, integrated absorbance of the F−C−F infrared band as a function of time. The infrared data were fit to the three-element viscoelastic relaxation model, with the relaxation time constant, β, as the only adjustable parameter. Note that the solution-cast Nafion membranes were, on average, thinner than the extruded Nafion 117 membranes (e.g., ≈100 μm vs ≈200 μm), and as such, the data collection time for these films was shorter (e.g., ≈300 s vs ≈1500 s). A summary of the relaxation model analysis for solution-cast Nafion and Nafion-SiNP membranes is presented in Table 1.

As seen in Table 1, the relaxation dynamics of the annealed Nafion membranes were ∼3-fold higher than that of the unannealed membranes. This result is in stark contrast to results obtained for extruded Nafion 117 membranes. The higher "stiffness" of the unannealed membrane may be due to the solution casting procedure utilized for membrane fabrication, as the membranes that form from this fabrication method are often thought of as being in a nonequilibrium state. That is, the dense membrane formed after solvent evaporation may lead to a more "frustrated" nanostructure for the Nafion membranes, which becomes more "relaxed" during thermal treatment of the membrane. This has been previously observed in a number of nanophase-segregated block copolymer systems, where solution-cast (or spun-cast) membranes are typically subject to long periods of thermal annealing.[55−60] This effect may be further heightened by the fact that the membrane adheres to the ATR crystal, introducing mechanical constraint on one side of the membrane. More specifically, it introduces mechanical constraint on the same side of the membrane where the absorbance data are being measured (i.e., at the polymer−ATR crystal interface, where the depth of penetration is ≈1 μm).[52,61] In this case, the annealing procedure provides enough energy to allow the Nafion chains to "flow" into a less frustrated structure.[45]

Comparing unannealed Nafion to its nanocomposite counterpart, we see that the introduction of 4% (by mass) SiO_2 results in ≈70% increase in the value of β_{norm} of the nanocomposite membrane. This result could indicate that the introduction of NPs alters how the Nafion chains pack during the solvent evaporation process. Interestingly, annealing these membranes resulted in only a slight reduction in the value of β_{norm} for the resultant annealed nanocomposite membrane. If we compare annealed Nafion to its nanocomposite counterpart, we see that the introduction of 4% (by mass) SiO_2 results in ≈60% decrease in the value of β_{norm}, indicating that the swelling dynamics of the nanocomposite membrane are slower than that of the annealed Nafion membranes. This is further highlighted if we compare annealed Nafion to membranes containing 10% (by mass) SiO_2, where the value for β_{norm} for these nanocomposites is ≈300% lower than that of the annealed Nafion. This result follows with previous studies which have reported reductions in membrane dynamics with increases in inorganic nanofillers.[11,17,19−21,23,62,63] Surprisingly, we only observe a slight reduction in the value of β_{norm} for the annealed membranes when the fraction of SiO_2 was increased from 4% to 10% (by mass), where the values of β_{norm} for unannealed Nafion and Nafion containing 10% (by mass) SiO_2 were equivalent.

Similar to what we observed with the extruded Nafion 117 membranes, the values of β_{norm} track well with the vanadium ion permeability values previously reported.[1] That is, the vanadium ion permeability was determined to be ≈60% higher in annealed Nafion membranes as compared to those that were annealed and contained 4% (by mass) SiO_2 (8.4×10^{-9} cm^2/s vs 5.3×10^{-9} cm^2/s). As seen from Table 1, the value for β_{norm} is ≈150% higher for annealed Nafion membranes when compared to their 4% (by mass) SiO_2 counterpart. Results from our current investigation suggest that the observed reduction in vanadium ion permeability with the introduction of SiNPs (at least for annealed, solution-cast membranes) may be due to a combined mechanism of increased stiffening of the polymer network as well as interaction of the SiNPs with the sulfonic acid groups of Nafion.

It has been previously postulated that SiNPs may restrict access of the vanadium ions to the sulfonic sites within the ionic channels by adhering to the channel walls, thereby impeding the permeation of vanadium ions through the ionomer membrane.[7] Notably, the authors report an insignificant impact of this interaction on proton transport, concurrent with other similar studies where increased water uptake in these nanocomposites was attributed to the offset in proton conductivity.[7,12,29] The engagement of sulfonic acid groups at the Nafion−NP interface due to electrostatic interactions can be correlated (at least qualitatively) to variations in the ion exchange capacity (IEC) of the nanocomposites. With regards to this, Jansto and Davis[13] observed ≈11% reduction in the IEC of Nafion when unfunctionalized (bare) SiNPs were added to the ionomer (5% (by mass) SiO_2). In addition, the reported variations in IEC with changes in surface functionalization of the SiNP was consistent with the notion that these particles directly interact with the pendant sulfonic acid groups in solution-cast Nafion nanocomposite membranes. Separately, Adjemian et al.[18] posited similar interactions between titania nanoparticles and the sulfonic groups in Nafion to explain observations involving thermal decomposition and mass spectroscopy studies on a series of Nafion−titania nanocomposites. Additionally, the researchers argued that particle dispersion (which is itself affected by processing technique, i.e., sol−gel vs solution-casting) influences the degree of engagement of sulfonic groups, though this impact is diminished at higher particle loading where agglomeration dominates.[64]

When we compare the values of β_{norm} between the two synthesis methods, we observe quite different trends between the different ionomer membranes. First, we see that for solution-cast membranes the value of β_{norm} actually increases after the Nafion membrane is annealed, which is opposite to what we observe for the extruded Nafion 117 membranes. Again, we hypothesize this is due to the solution casting method, whereby the as-cast, unannealed membranes have a more "frustrated" structure that is relaxed by annealing the membrane, resulting in an increase in membrane swelling dynamics. However, we do observe a similar trend for both fabrication methods with the introduction of 4% (by mass) SiO_2 to the annealed Nafion membranes, where these nanocomposite membranes showed a large decrease in the value of β_{norm} compared to those membranes that had only received thermal annealing (i.e., annealed with no SiNPs). We again see a different trend for the different fabrication techniques when the fraction of SiNPs is increased from 4% to 10% (by mass). We believe the contrasting trends in the calculated relaxation dynamics may be indicative of the

DOI: 10.1021/acs.macromol.8b02189
Macromolecules 2019, 52, 2120−2130

different mechanisms by which the SiO_2 phase is introduced into the ionomer membrane.

As previously noted, the silica phase within the two series of membranes may be quite different due to the two different fabrication methods. Sahu et al.[65] note a marked change in structural arrangement of SiO_2 phase toward a more linear conformation with increasing acid content (such as available within Nafion), when the nanocomposites are prepared via the sol−gel method. Additionally, an FTIR study of evolution of silica morphology within the ionomer matrix suggests that an increase in concentration of silica precursor drives the silica morphology from a cyclical network to more linear/extended network.[2] In the case of sol−gel synthesized membranes, the silica precursor solution is the more mobile phase, as it has the freedom to assemble and nucleate around the pre-existing sulfonic clusters as it penetrates the Nafion membrane. This assembly can be heavily constrained by the fluorocarbon network and is understood to resolve to a linear network at higher concentrations to minimize conformational energy.

Alternatively, in the case of solution-cast membranes, the discrete, preformed SiNPs as well as the solvated ionomer chains can be considered mobile phases within the dispersion (solution). However, the kinetics of assembly are constrained by the entanglement effects of chains under increasing concentration (i.e., as the solvent evaporates). Thus, the resulting morphology and dispersion of NPs within the resultant nanocomposite may deviate from an "equilibrium state", as the formation of the final dense membrane is governed by the rate of solvent evaporation. From these two contrasting pictures, it seems plausible that the mechanism by which SiNPs act to alter viscoelastic swelling properties of the polymer may be quite different, resulting in different trends at higher silica content (e.g., ≈10% (by mass) SiO_2). The structure (and dispersion) of the silica phase formed via solution-casting can be seen in TEM images from our recent investigations on analogous membranes and SiNPs. Unlike the percolated network of silica that is expected within composite membranes formed via the sol−gel technique, membranes formed using solution-casting method are shown to have discrete aggregate structures.[2,13]

Note that differences in trends in the values of β_{norm} between extruded and solution-cast membranes may be due to differences in the how the ionomer membranes "respond" to the diffusion of water through the membrane. Previous reports in the literature indicate that major structural reorganization takes place while Nafion undergoes hydration, where in general water-saturated hydrophilic domains exert significant forces on the hydrophobic domains.[66−69] We postulate that our polymer relaxation data captures a difference in the reorganization kinetics between the two fabrication techniques. For extruded Nafion membranes, we capture an initial "pseudoequilibrium" in the ionomer swelling data that was previously masked when the frequency of absorbance data collection was too low (i.e., long time between collection of each data point).

As seen in Figure 4, we observe a plateau around 100 s in the relaxation data for the extruded Nafion membranes, indicating an initial "short time" reorganization of the Nafion nanostructure, followed by a longer term, potentially longer range, reorganization of the membrane (seen in longer experiments shown in Figure 2). Additionally, when this "short time" data is fit to eq 1, we observe that the relaxation dynamics are faster than what we calculate when the "long time" data is fit to the relaxation model (compare Figures 4 and 2a). Specifically, we observed an ≈25% increase in the value of β_{norm} when only analyzing the short time data (for "short time" experiment, $\beta_{norm} = (13.93 \pm 1.45) \times 10^{-6}$ cm^2/s vs $\beta_{norm} = (11.1 \pm 2) \times 10^{-6}$ cm^2/s for repeat "long time" experiments). Surprisingly, over the time scale of interest for this discussion, we do not observe such a "pseudoequilibrium" in the swelling data for solution-cast Nafion. Again, we believe the absence of this "short time" plateau is related to differences in the reorganization mechanism between the extruded and solution-cast membranes. These multiple time scales we capture may also provide information regarding how the SiNPs are partitioned in the ionomer membrane, which will be the scope of our future studies.

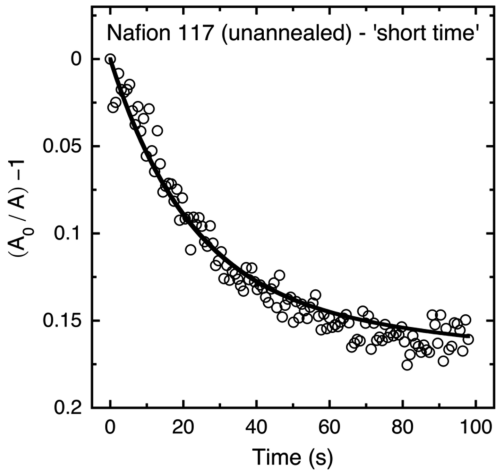

Figure 4. "Short time" time-resolved absorbance data of the polymer backbone CF_2 stretching as a function of time at 25 °C for extruded, unannealed Nafion 117. The solid lines represent the full solution of eq 1, where relaxation time constant (β) was the only adjustable fitting parameter. Note that only 50% of the time-resolved data are being shown for clarity. The thermal treatment conditions of all the samples are indicated (in parentheses) next to the sample name.

Segmental Dynamics of Ionomer Nanocomposites. To gain insight into the impact of the SiO_2 phase on the segmental relaxation dynamics of the Nafion−SiO_2 nanocomposite membranes, neutron spin echo (NSE) spectrometry was employed. Unlike elastic neutron scattering techniques (e.g., small-angle neutron scattering or SANS), NSE is a quasielastic neutron scattering method, which provides a measurement of the structural dynamics within polymer systems over large ranges of length and time scales. Figure 5 shows the NSE curves collected in correspondence of the sample structure factor peak, $Q = 1.2$ Å^{-1} or $Q = 1.3$ Å^{-1} (Q being the exchanged wavevector, which in this particular case, corresponds to the length scale of fluorocarbon chain packing), for both sol−gel synthesized (Figures 5a and 5b) and solution-cast Nafion and Nafion nanocomposite (Figure 5c) membranes at 25 °C. Note that the membranes were equilibrated in liquid D_2O for a period of 24 h prior to beginning experiments.

Specifically, Figure 5 shows the intermediate structure factor for each series of Nafion membranes as a function of time, where the length scales correlating to the packing order of fluorocarbon were probed to interpret effect of changes in crystallinity and silica content on the segmental dynamics in the hydrophobic phase. Traditionally, the data in Figure 5 are best represented by a stretched exponential function (in context of relaxation in disordered polymeric systems, the

DOI: 10.1021/acs.macromol.8b02189
Macromolecules 2019, 52, 2120−2130

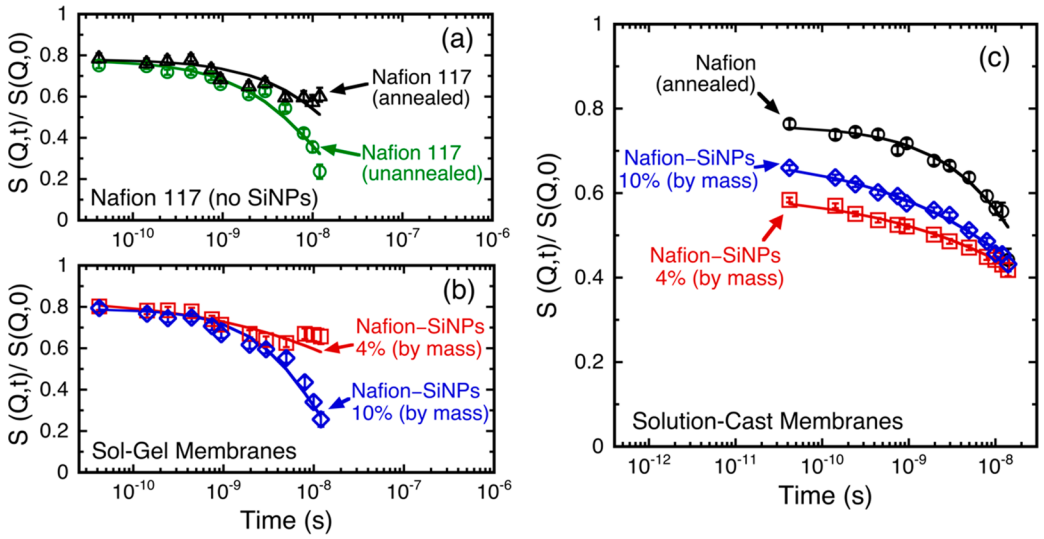

Figure 5. Neutron spin echo (NSE) data (intermediate structure factor as a function of time) for (a) neat, unannealed (open green triangles) and annealed (open black circles) Nafion 117 membranes, (b) annealed Nafion 117 membranes with 4% (by mass) SiO_2 (open red squares) and 13% (by mass) SiO_2 (open blue diamonds) prepared by sol–gel method, and (c) solution-cast, annealed Nafion with no SiNPs (open black circles), 4% (by mass) SiO_2 (open red squares), and 10% (by mass) SiO_2 (open blue diamonds). The solid lines are a best fit of the NSE data to the KWW model (eq 2). All membranes were equilibrated in D_2O. All NSE data were collected at T = 298 K and Q = 1.2 $Å^{-1}$ (sol–gel samples) and 1.3 $Å^{-1}$ (solution-cast samples). The thermal treatment conditions of all the samples are indicated (in parentheses) next to the sample name.

Table 2. Model Parameters Obtained from a Regression of the NSE Data to the KWW Equation (Eq 2)[a]

membrane	pre-exponential constant [A]	stretching exponent [α]	characteristic segmental relaxation time [t_R] (ns)	average segmental relaxation time [$\langle t_R \rangle$] (ns)
sol–gel membranes				
Nafion 117 (unannealed)	0.78 ± 0.01	0.76 ± 0.03	14.2 ± 1.0	16.7 ± 1.4
Nafion 117 (annealed)	0.78 ± 0.03	0.76 ± 0.09	37.1 ± 1.5	43.7 ± 5.5
Nafion–SiO_2 nanocomposite, 4% (by mass) SiO_2 (annealed)	0.84 ± 0.01	0.37 ± 0.01	175 ± 55	731 ± 234
Nafion–SiO_2 nanocomposite, 13% (by mass) SiO_2 (annealed)	0.79 ± 0.01	0.95 ± 0.05	11.2 ± 0.6	11.5 ± 0.9
solution-cast membranes				
Nafion (annealed)	0.76 ± 0.01	0.66 ± 0.02	60.2 ± 2.7	80.9 ± 4.4
Nafion–SiO_2 nanocomposite, 4% (by mass) SiO_2 (annealed)	0.61 ± 0.03	0.32 ± 0.05	370 ± 17	2600 ± 1270
Nafion–SiO_2 nanocomposite, 10% (by mass) SiO_2 (annealed)	0.69 ± 0.02	0.35 ± 0.05	140 ± 34	706 ± 367

[a]The thermal treatment conditions of all the samples are indicated (in parentheses) next to the sample name.

Kohlrausch–Williams–Watts (KWW) equation).[47] The KWW equation is as follows:

$$\frac{S(Q,t)}{S(Q,0)} = A \exp\left[-\left(\frac{t}{t_R}\right)^{\alpha}\right] \quad (2)$$

where $S(Q,t)$ and $S(Q,0)$ are the intermediate structure factors (ISFs) at time t and at time t = 0, respectively, A is the pre-exponential factor, and t_R is the segmental relaxation time. The exponential, α, indicates the degree of inhomogeneity in the segment population being probed and is a mathematical parameter that "stretches" the exponential decay, indicating cooperative dynamics between different segments of the polymer chain (for general polymeric systems, $\alpha \approx 0.5$).[47,70] The solid lines in Figure 5a–c represent a best fit of the NSE data to the KWW model (eq 2). The values of the pre-exponential factor, the stretching exponent, and the segmental relaxation time obtained from this regression are listed in Table 2. From Figure 5 and Table 2, we see that the incorporation of SiO_2 results in an observable slowdown in the relaxation dynamics of the local chains. Note that a nonunity value of the pre-exponent factor (A) signifies that there are segmental dynamics at shorter time scales. However, interpretation of NSE data at these smaller time scales is beyond the scope of this study and will be analyzed in greater detail in a forthcoming investigation.

As seen from Table 2, the stretching exponent, α, varies from a value of ≈0.32 to ≈0.95. Note that at these length and time scales the rigid crystalline domains in the ionomer membranes have no time-dependent fluctuations. As such, these domains introduce a constant background in the ISF associated with the immobile segments, which would be reflected with higher relaxation times and, typically, increased stretching. Given this, it is more accurate to compare values of the average relaxation time for each membrane. By use of the values for α and t_R, the average relaxation time for each ionomer membrane can be calculated using the equation

$$\langle t_R \rangle = \frac{t_R}{\alpha}\Gamma\left(\frac{1}{\alpha}\right) \quad (3)$$

DOI: 10.1021/acs.macromol.8b02189
Macromolecules 2019, 52, 2120–2130

where $\langle t_R \rangle$ is the average segmental relaxation time and $\Gamma(1/\alpha)$ is the gamma function of $1/\alpha$. The segmental dynamics of the Nafion, both sol−gel synthesized and solution-cast, are significantly hindered with the introduction of just 4% (by mass) SiO_2. For solution-cast samples, the average segmental relaxation time increases from a value of $\langle t_R \rangle$ = 80.9 ± 4.4 ns for annealed membranes to a value of $\langle t_R \rangle$ = 2600 ± 1270 ns for membranes with 4% (by mass) SiNPs. Similarly, for nanocomposites synthesized via the sol−gel method, the average segmental relaxation time increases from a value of $\langle t_R \rangle$ = 43.7 ± 5.5 ns for annealed membranes to a value of $\langle t_R \rangle$ = 731 ± 234 ns for membranes with 4% (by mass) SiNPs. Note that, as the experimental time scale was on the order of tens of nanoseconds, values for the average segmental relaxation time above hundreds of nanoseconds cannot be taken as quantitatively accurate. The discrepancy between experimental time scale and resulting average relaxation times is directly reflected in the uncertainties on these values for membranes with 4% (by mass) SiNPs. However, despite these large uncertainties, qualitative inferences regarding the slow-down in segmental dynamics due to incorporation of nanoparticles at this concentration hold, as can be seen in Figure 5c, where the intermediate structure factors for these samples show the slowest decay with time. Surprisingly, for both series, when the SiO_2 loading was increased to 10% (by mass), the average segmental relaxation time decreased from that observed for Nafion membranes containing 4% (by mass) SiO_2.

As seen in Table 2, the average segmental relaxation time for the solution-cast membranes decreases by ≈70% to a value of $\langle t_R \rangle$ = 706 ± 367 ns when the SiNP loading is increased from 4% (by mass) to 10% (by mass) SiO_2. However, the segmental relaxation time is still over 800% greater than that of the annealed Nafion membrane with no SiNPs. Similarly, for sol−gel nanocomposite films, when the loading of the SiO_2 phase is increased to ≈13% (by mass), we observe a significant decrease in the average segmental relaxation time to a value of $\langle t_R \rangle$ = 11.5 ± 0.9 ns. However, unlike solution-cast membranes, the segmental relaxation time is over an order of magnitude faster when compared to membranes with 4% (by mass) SiO_2 and is equivalent to the segmental dynamics of an unannealed, unmodified Nafion membrane.

Previous FTIR analysis of the evolution of a 3-dimensional silica network within Nafion for sol−gel synthesized Nafion 117 membranes performed by Mauritz et al.[2] indicated that the network structure/distribution of the silica phase transitioned from a cyclic, more cross-linked network to a reduced linear network as the SiO_2 concentration was increased from 3% (by mass) to 10% (by mass). Furthermore, Deng and co-workers have suggested that for Nafion−SiO_2 nanocomposites formed via the sol−gel method the main-chain dynamics of Nafion are coupled to the side-chain mobility, and these dynamics are hindered when the side chains are tethered to silicon oxide nanophases.[71] Alternatively, for a Nafion nanocomposite containing titania NPs, Majsztrik et al.[64] observed that both NP size and NP loading affect the NP−Nafion interactions. Specifically, use of particles with larger surface area showed a greater degree of interaction between sulfonic groups and resulted in better thermal stability of the composite. In addition, the degree of interaction was seen to improve up to nanoparticles loadings of 6% (by mass), although nanoparticle agglomeration at higher loadings, notably, at 20% (by mass), resulted in a deterioration of these interactions. Thus, it is plausible that a similar behavior is reproduced with SiNPs in the NSE experiments and presents an alternate possibility that SiNPs are dispersed at the interface of long chain Teflon- and short-chain ionic phases in solution-cast Nafion−SiNP nanocomposites.

While previously discussed scattering studies establish a significant mismatch between the length scales of inorganic silica phases and ionic channels within these ionomer composites, it is possible that the growth of this phase is nucleated at the ionic sites and impinges on the swollen hydrophobic backbone. In light of this assumption, the changes in the stretching exponents for sol−gel samples (Table 2) can be interpreted as increased heterogeneity in the fluorocarbon phase (i.e., silica nanoparticles are not impacting the bulk membrane homogeneously). For 10% (by mass) modified Nafion−SiO_2 samples, $\alpha \approx 1$ could suggest a significant perturbation of backbone dynamics with the increased presence of SiO_2 phase. For instance, a complete decoupling of the amorphous backbone chain dynamics from the silica network could allow the sample to recover behavior of as-used, unmodified Nafion membrane. However, a more exhaustive investigation is required to confirm this hypothesis and also explain a similar behavior observed for solution-cast films, where the particles and Nafion chains have a significantly higher conformational entropy compared to the preformed, extruded Nafion 117 membranes. That is, the Nafion chains, and thus the Nafion nanostructure, have higher degrees of freedom to arrange and minimize any thermodynamically unfavorable interactions during membrane formation (i.e., during solvent evaporation).

■ CONCLUSIONS

In summary, the local segmental relaxation dynamics, as well as the bulk swelling dynamics of two series of Nafion nanocomposites, one synthesized via the sol−gel method and the other via solution casting, was measured using NSE and *t*ATR-FTIR spectroscopy, respectively. Ionomer swelling/rearrangement data (i.e., dilution of the F−C−F infrared band with time due to the diffusion of liquid water) obtained from *t*ATR-FTIR measurements were fit to a three-element viscoelastic model to obtain swelling (relaxation) time constants, which indicated stiffening of polymer chains with the introduction of just 4% (by mass) SiO_2. These trends were congruent with changes in the local segmental dynamics as measured by NSE spectroscopy, where a curious increase in the segmental dynamics was observed at higher silica loadings (10% (by mass) SiO_2) for both solution-cast and sol−gel synthesized membranes. Presently, the data suggest that SiNPs reside at the interface of hydrophobic and hydrophilic domains and may act to impede vanadium swelling by a stiffening of the ionic network.

■ AUTHOR INFORMATION

Corresponding Author

*E-mail: ericd@clemson.edu.

ORCID

Eric M. Davis: 0000-0002-5633-5489

Notes

The authors declare no competing financial interest.

■ ACKNOWLEDGMENTS

This research was funded by Clemson University Department of Chemical and Biomolecular Engineering start-up funds.

DOI: 10.1021/acs.macromol.8b02189
Macromolecules 2019, 52, 2120−2130

Access to the neutron spin echo spectrometer was provided by the Center for High Resolution Neutron Scattering, which is a partnership between the National Institute of Standards and Technology and the National Science Foundation under Grant DMR-1508249. Certain commercial equipment, instruments, or materials (or suppliers, or software, etc.) are identified in this paper to foster understanding. Such identification does not imply recommendation or endorsement by the National Institute of Standards and Technology, nor does it imply that the materials or equipment identified are necessarily the best available for the purpose.

REFERENCES

(1) Davis, E. M.; Kim, J.; Oleshko, V. P.; Page, K. A.; Soles, C. L. Uncovering the Structure of Nafion-SiO $_2$ Hybrid Ionomer Membranes for Prospective Large-Scale Energy Storage Devices. *Adv. Funct. Mater.* **2015**, *25* (26), 4064−4075.

(2) Mauritz, K. A.; Warren, R. M. Microstructural Evolution of a Silicon Oxide Phase in a Perfluorosulfonic Acid Ionomer by an in Situ Sol-Gel Reaction. 1. Infrared Spectroscopic Studies. *Macromolecules* **1989**, *22* (4), 1730−1734.

(3) Miyake, N.; Wainright, J. S.; Savinell, R. F. Evaluation of a Sol-Gel Derived Nafion/Silica Hybrid Membrane for Proton Electrolyte Membrane Fuel Cell Applications: I. Proton Conductivity and Water Content. *J. Electrochem. Soc.* **2001**, *148* (8), A898−A904.

(4) Zhang, H.; Zhang, H.; Li, X.; Mai, Z.; Wei, W. Silica Modified Nanofiltration Membranes with Improved Selectivity for Redox Flow Battery Application. *Energy Environ. Sci.* **2012**, *5* (4), 6299−6303.

(5) Sum, E.; Skyllas-Kazacos, M. A Study of the V(II)/V(III) Redox Couple for Redox Flow Cell Applications. *J. Power Sources* **1985**, *15* (2), 179−190.

(6) Jang, S. S.; Molinero, V.; Çağın, T.; Goddard, W. A. Nanophase-Segregation and Transport in Nafion 117 from Molecular Dynamics Simulations: Effect of Monomeric Sequence. *J. Phys. Chem. B* **2004**, *108* (10), 3149−3157.

(7) Schwenzer, B.; Zhang, J.; Kim, S.; Li, L.; Liu, J.; Yang, Z. Membrane Development for Vanadium Redox Flow Batteries. *ChemSusChem* **2011**, *4* (10), 1388−1406.

(8) Teng, X.; Zhao, Y.; Xi, J.; Wu, Z.; Qiu, X.; Chen, L. Nafion/Organically Modified Silicate Hybrids Membrane for Vanadium Redox Flow Battery. *J. Power Sources* **2009**, *189* (2), 1240−1246.

(9) Chung, K.-S.; Kim, S.-K.; Jung, D.-H.; Choi, S.-Y.; Lee, S.; Lee, J.-W.; Kim, T.; Peck, D.-H. Effects of Silicon Dioxide on the High-Temperature Performance of Polymer/Ceramic Composite Membranes for Direct Methanol Fuel Cells. *Nanosci. Nanotechnol. Lett.* **2017**, *9* (1), 30−34.

(10) Dresch, M. A.; Matos, B. R.; Fonseca, F. C.; Santiago, E. I.; Carmo, M.; Lanfredi, A. J. C.; Balog, S. Small-Angle X-Ray and Neutron Scattering Study of Nafion-SiO_2 Hybrid Membranes Prepared in Different Solvent Media. *J. Power Sources* **2015**, *274*, 560−567.

(11) Ghassemzadeh, L.; Pace, G.; Di Noto, V.; Müller, K. Effect of SiO_2 on the Dynamics of Proton Conducting [Nafion/(SiO_2)X] Composite Membranes: A Solid-State 19F NMR Study. *Phys. Chem. Chem. Phys.* **2011**, *13* (20), 9327.

(12) Jiang, R.; Kunz, H. R.; Fenton, J. M. Composite Silica/Nafion® Membranes Prepared by Tetraethylorthosilicate Sol−Gel Reaction and Solution Casting for Direct Methanol Fuel Cells. *J. Membr. Sci.* **2006**, *272* (1), 116−124.

(13) Jansto, A.; Davis, E. M. Role of Surface Chemistry on Nanoparticle Dispersion and Vanadium Ion Crossover in Nafion Nanocomposite Membranes. *ACS Appl. Mater. Interfaces* **2018**, *10*, 36385.

(14) Schulte, D.; Drillkens, J.; Schulte, B.; Sauer, D. U. Nafion Hybrid Membranes for Use in Redox Flow Batteries. *J. Electrochem. Soc.* **2010**, *157* (9), A989−A992.

(15) Mauritz, K. A.; Stefanithis, I. D. Microstructural Evolution of a Silicon Oxide Phase in a Perfluorosulfonic Acid Ionomer by an in Situ Sol-Gel Reaction. 2. Dielectric Relaxation Studies. *Macromolecules* **1990**, *23* (5), 1380−1388.

(16) Stefanithis, I. D.; Mauritz, K. A. Microstructural Evolution of a Silicon Oxide Phase in a Perfluorosulfonic Acid Ionomer by an in Situ Sol-Gel Reaction. 3. Thermal Analysis Studies. *Macromolecules* **1990**, *23* (8), 2397−2402.

(17) Di Noto, V.; Gliubizzi, R.; Negro, E.; Pace, G. Effect of SiO_2 on Relaxation Phenomena and Mechanism of Ion Conductivity of [Nafion/(SiO_2)x] Composite Membranes. *J. Phys. Chem. B* **2006**, *110* (49), 24972−24986.

(18) Adjemian, K. T.; Dominey, R.; Krishnan, L.; Ota, H.; Majsztrik, P.; Zhang, T.; Mann, J.; Kirby, B.; Gatto, L.; Velo-Simpson, M.; et al. Function and Characterization of Metal Oxide−Nafion Composite Membranes for Elevated-Temperature H2/O2 PEM Fuel Cells. *Chem. Mater.* **2006**, *18* (9), 2238−2248.

(19) Bansal, A.; Yang, H.; Li, C.; Benicewicz, B. C.; Kumar, S. K.; Schadler, L. S. Controlling the Thermomechanical Properties of Polymer Nanocomposites by Tailoring the Polymer−Particle Interface. *J. Polym. Sci., Part B: Polym. Phys.* **2006**, *44* (20), 2944−2950.

(20) Akcora, P.; Kumar, S. K.; Moll, J.; Lewis, S.; Schadler, L. S.; Li, Y.; Benicewicz, B. C.; Sandy, A.; Narayanan, S.; Ilavsky, J.; et al. Gel-like" Mechanical Reinforcement in Polymer Nanocomposite Melts. *Macromolecules* **2010**, *43* (2), 1003−1010.

(21) Bogoslovov, R. B.; Roland, C. M.; Ellis, A. R.; Randall, A. M.; Robertson, C. G. Effect of Silica Nanoparticles on the Local Segmental Dynamics in Poly(Vinyl Acetate). *Macromolecules* **2008**, *41* (4), 1289−1296.

(22) Fragiadakis, D.; Pissis, P.; Bokobza, L. Glass Transition and Molecular Dynamics in Poly(Dimethylsiloxane)/Silica Nanocomposites. *Polymer* **2005**, *46* (16), 6001−6008.

(23) Narayanan, R. A.; Thiyagarajan, P.; Lewis, S.; Bansal, A.; Schadler, L. S.; Lurio, L. B. Dynamics and Internal Stress at the Nanoscale Related to Unique Thermomechanical Behavior in Polymer Nanocomposites. *Phys. Rev. Lett.* **2006**, *97* (7), 075505.

(24) Casciola, M.; Capitani, D.; Donnadio, A.; Frittella, V.; Pica, M.; Sganappa, M. Preparation, Proton Conductivity and Mechanical Properties of Nafion 117-Zirconium Phosphate Sulphophenylphosphonate Composite Membranes. *Fuel Cells* **2009**, *9* (4), 381−386.

(25) Hassan, M. K.; Abukmail, A.; Mauritz, K. A. Broadband Dielectric Spectroscopic Studies of Molecular Motions in a Nafion® Membrane vs. Annealing Time and Temperature. *Eur. Polym. J.* **2012**, *48* (4), 789−802.

(26) Kyu, T.; Eisenberg, A. Mechanical Relaxations in Perfluorosulfonate Ionomer Membranes. In *Perfluorinated Ionomer Membranes*; ACS Symposium Series; American Chemical Society: 1982; Vol. *180*, pp 79−110.

(27) Di Noto, V.; Boaretto, N.; Negro, E.; Pace, G. New Inorganic−Organic Proton Conducting Membranes Based on Nafion and Hydrophobic Fluoroalkylated Silica Nanoparticles. *J. Power Sources* **2010**, *195* (23), 7734−7742.

(28) Kumar Mishra, A.; Kuila, T.; Kim, D.-Y.; Hoon Kim, N.; Hee Lee, J. Protic Ionic Liquid -Functionalized Mesoporous Silica-Based Hybrid Membranes for Proton Exchange Membrane Fuel Cells. *J. Mater. Chem.* **2012**, *22* (46), 24366−24372.

(29) Kim, J.-H.; Kim, S.-K.; Nam, K.; Kim, D.-W. Composite Proton Conducting Membranes Based on Nafion and Sulfonated SiO_2 Nanoparticles. *J. Membr. Sci.* **2012**, *415−416*, 696−701.

(30) Staiti, P.; Aricò, A. S.; Baglio, V.; Lufrano, F.; Passalacqua, E.; Antonucci, V. Hybrid Nafion−Silica Membranes Doped with Heteropolyacids for Application in Direct Methanol Fuel Cells. *Solid State Ionics* **2001**, *145* (1), 101−107.

(31) Antonucci, P. L.; Aricò, A. S.; Cretì, P.; Ramunni, E.; Antonucci, V. Investigation of a Direct Methanol Fuel Cell Based on a Composite Nafion®-Silica Electrolyte for High Temperature Operation. *Solid State Ionics* **1999**, *125* (1), 431−437.

(32) Shao, Z.-G.; Joghee, P.; Hsing, I.-M. Preparation and Characterization of Hybrid Nafion−Silica Membrane Doped with Phosphotungstic Acid for High Temperature Operation of Proton Exchange Membrane Fuel Cells. *J. Membr. Sci.* **2004**, *229* (1), 43−51.

DOI: 10.1021/acs.macromol.8b02189
Macromolecules 2019, 52, 2120−2130

(33) Hickner, M. A. Water-Mediated Transport in Ion-Containing Polymers. *J. Polym. Sci., Part B: Polym. Phys.* **2012**, *50* (1), 9−20.
(34) Wang, Y.; Agapov, A. L.; Fan, F.; Hong, K.; Yu, X.; Mays, J.; Sokolov, A. P. Decoupling of Ionic Transport from Segmental Relaxation in Polymer Electrolytes. *Phys. Rev. Lett.* **2012**, *108* (8), 088303.
(35) Spohr, E.; Commer, P.; Kornyshev, A. A. Enhancing Proton Mobility in Polymer Electrolyte Membranes: Lessons from Molecular Dynamics Simulations. *J. Phys. Chem. B* **2002**, *106* (41), 10560−10569.
(36) Dura, J. A.; Murthi, V. S.; Hartman, M.; Satija, S. K.; Majkrzak, C. F. Multilamellar Interface Structures in Nafion. *Macromolecules* **2009**, *42* (13), 4769−4774.
(37) Damasceno Borges, D.; Gebel, G.; Franco, A. A.; Malek, K.; Mossa, S. Morphology of Supported Polymer Electrolyte Ultrathin Films: A Numerical Study. *J. Phys. Chem. C* **2015**, *119* (2), 1201−1216.
(38) Modestino, M. A.; Kusoglu, A.; Hexemer, A.; Weber, A. Z.; Segalman, R. A. Controlling Nafion Structure and Properties via Wetting Interactions. *Macromolecules* **2012**, *45* (11), 4681−4688.
(39) Kusoglu, A.; Kushner, D.; Paul, D. K.; Karan, K.; Hickner, M. A.; Weber, A. Z. Impact of Substrate and Processing on Confinement of Nafion Thin Films. *Adv. Funct. Mater.* **2014**, *24* (30), 4763−4774.
(40) Akcora, P.; Kumar, S. K.; García Sakai, V.; Li, Y.; Benicewicz, B. C.; Schadler, L. S. Segmental Dynamics in PMMA-Grafted Nanoparticle Composites. *Macromolecules* **2010**, *43* (19), 8275−8281.
(41) Gagliardi, S.; Arrighi, V.; Ferguson, R.; Telling, M. T. F. Restricted Dynamics in Polymer-Filler Systems. *Phys. B* **2001**, *301* (1), 110−114.
(42) Polymer−nanoparticle interfacial interactions in polymer nanocomposites: Confinement effects on glass transition temperature and suppression of physical aging - Rittigstein - 2006 - Journal of Polymer Science Part B: Polymer Physics - Wiley Online Library; http://onlinelibrary.wiley.com/doi/10.1002/polb.20925/full. (accessed Nov 29, 2017).
(43) Fragiadakis, D.; Pissis, P. Glass Transition and Segmental Dynamics in Poly(Dimethylsiloxane)/Silica Nanocomposites Studied by Various Techniques. *J. Non-Cryst. Solids* **2007**, *353* (47), 4344−4352.
(44) Bansal, A.; Yang, H.; Li, C.; Cho, K.; Benicewicz, B. C.; Kumar, S. K.; Schadler, L. S. Quantitative Equivalence between Polymer Nanocomposites and Thin Polymer Films. *Nat. Mater.* **2005**, *4* (9), 693−698.
(45) Page, K. A.; Cable, K. M.; Moore, R. B. Molecular Origins of the Thermal Transitions and Dynamic Mechanical Relaxations in Perfluorosulfonate Ionomers. *Macromolecules* **2005**, *38* (15), 6472−6484.
(46) Hallinan, D. T.; De Angelis, M. G.; Giacinti Baschetti, M.; Sarti, G. C.; Elabd, Y. A. Non-Fickian Diffusion of Water in Nafion. *Macromolecules* **2010**, *43* (10), 4667−4678.
(47) Page, K. A.; Rowe, B. W.; Masser, K. A.; Faraone, A. The Effect of Water Content on Chain Dynamics in Nafion Membranes Measured by Neutron Spin Echo and Dielectric Spectroscopy. *J. Polym. Sci., Part B: Polym. Phys.* **2014**, *52* (9), 624−632.
(48) Hallinan, D. T.; Elabd, Y. A. Diffusion of Water in Nafion Using Time-Resolved Fourier Transform Infrared−Attenuated Total Reflectance Spectroscopy. *J. Phys. Chem. B* **2009**, *113* (13), 4257−4266.
(49) Azuah, R. T.; Kneller, L. R.; Qiu, Y.; Tregenna-Piggott, P. L. W.; Brown, C. M.; Copley, J. R. D.; Dimeo, R. M. DAVE: A Comprehensive Software Suite for the Reduction, Visualization, and Analysis of Low Energy Neutron Spectroscopic Data. *J. Res. Natl. Inst. Stand. Technol.* **2009**, *114* (6), 341−358.
(50) Gruger, A.; Régis, A.; Schmatko, T.; Colomban, P. Nanostructure of Nafion® Membranes at Different States of Hydration: An IR and Raman Study. *Vib. Spectrosc.* **2001**, *26* (2), 215−225.
(51) Hallinan, D.; Grazia De Angelis, M.; Giacinti Baschetti, M.; Sarti, G.; Elabd, Y. A. *ECS Trans.* **2010**, 1029−1033.
(52) Elabd, Y. A.; Baschetti, M. G.; Barbari, T. A. Time-Resolved Fourier Transform Infrared/Attenuated Total Reflection Spectroscopy for the Measurement of Molecular Diffusion in Polymers. *J. Polym. Sci., Part B: Polym. Phys.* **2003**, *41* (22), 2794−2807.
(53) Davis, E. M.; Benetatos, N. M.; Regnault, W. F.; Winey, K. I.; Elabd, Y. A. The Influence of Thermal History on Structure and Water Transport in Parylene C Coatings. *Polymer* **2011**, *52* (23), 5378−5386.
(54) Davis, E. M.; Stafford, C. M.; Page, K. A. Elucidating Water Transport Mechanisms in Nafion Thin Films. *ACS Macro Lett.* **2014**, *3* (10), 1029−1035.
(55) Mori, K.; Hasegawa, H.; Hashimoto, T. Ordered Structure in Block Polymer Solutions: 6. Possible Non-Equilibrium Effects on Growth of Self-Assembling Structures. *Polymer* **1990**, *31* (12), 2368−2376.
(56) O'Shaughnessy, B.; Vavylonis, D. Non-Equilibrium in Adsorbed Polymer Layers. *J. Phys.: Condens. Matter* **2005**, *17* (2), R63−R99.
(57) Li, R. N.; Clough, A.; Yang, Z.; Tsui, O. K. C. Equilibration of Polymer Films Cast from Solutions with Different Solvent Qualities. *Macromolecules* **2012**, *45* (2), 1085−1089.
(58) McGraw, J. D.; Fowler, P. D.; Ferrari, M. L.; Dalnoki-Veress, K. Relaxation of Non-Equilibrium Entanglement Networks in Thin Polymer Films. *Eur. Phys. J. E: Soft Matter Biol. Phys.* **2013**, *36* (1), 7.
(59) Tsuji, H.; Ikada, Y. Stereocomplex Formation between Enantiomeric Poly(Lactic Acid)s. XI. Mechanical Properties and Morphology of Solution-Cast Films. *Polymer* **1999**, *40* (24), 6699−6708.
(60) Eriksson, M.; Goossens, H.; Peijs, T. Influence of Drying Procedure on Glass Transition Temperature of PMMA Based Nanocomposites. *Nanocomposites* **2015**, *1* (1), 36−45.
(61) Santos, M. C.; Bendiksen, B.; Elabd, Y. A. Diffusion of Liquid Water in Free-Standing Polymer Films Using Pressure-Contact Time-Resolved Fourier Transform Infrared Attenuated Total Reflectance Spectroscopy. *Ind. Eng. Chem. Res.* **2017**, *56* (12), 3464−3476.
(62) Oh, H.; Green, P. F. Polymer Chain Dynamics and Glass Transition in Athermal Polymer/Nanoparticle Mixtures. *Nat. Mater.* **2009**, *8* (2), 139−143.
(63) Robertson, C. G.; Roland, C. M. Glass Transition and Interfacial Segmental Dynamics in Polymer-Particle Composites. *Rubber Chem. Technol.* **2008**, *81* (3), 506−522.
(64) Majsztrik, P. W. Mechanical and Transport Properties of Nafion® for PEM Fuel Cells; Temperature and Hydration Effects. PhD Thesis, Princeton University, Princeton, 2008.
(65) Sahu, A. K.; Selvarani, G.; Pitchumani, S.; Sridhar, P.; Shukla, A. K. A Sol-Gel Modified Alternative Nafion-Silica Composite Membrane for Polymer Electrolyte Fuel Cells. *J. Electrochem. Soc.* **2007**, *154* (2), B123−B132.
(66) Fumagalli, M.; Lyonnard, S.; Prajapati, G.; Berrod, Q.; Porcar, L.; Guillermo, A.; Gebel, G. Fast Water Diffusion and Long-Term Polymer Reorganization during Nafion Membrane Hydration Evidenced by Time-Resolved Small-Angle Neutron Scattering. *J. Phys. Chem. B* **2015**, *119* (23), 7068−7076.
(67) Rubatat, L.; Rollet, A. L.; Gebel, G.; Diat, O. Evidence of Elongated Polymeric Aggregates in Nafion. *Macromolecules* **2002**, *35* (10), 4050−4055.
(68) Kusoglu, A.; Modestino, M. A.; Hexemer, A.; Segalman, R. A.; Weber, A. Z. Subsecond Morphological Changes in Nafion during Water Uptake Detected by Small-Angle X-Ray Scattering. *ACS Macro Lett.* **2012**, *1* (1), 33−36.
(69) Kreuer, K.-D.; Portale, G. A Critical Revision of the Nano-Morphology of Proton Conducting Ionomers and Polyelectrolytes for Fuel Cell Applications. *Adv. Funct. Mater.* **2013**, *23* (43), 5390−5397.
(70) León, C.; Ngai, K. L. Rapidity of the Change of the Kohlrausch Exponent of the α-Relaxation of Glass-Forming Liquids at TB or Tβ and Consequences. *J. Phys. Chem. B* **1999**, *103* (20), 4045−4051.
(71) Deng, Q.; Moore, R. B.; Mauritz, K. A. Nafion®/(SiO_2, ORMOSIL, and Dimethylsiloxane) Hybrids via in Situ Sol−Gel Reactions: Characterization of Fundamental Properties. *J. Appl. Polym. Sci.* **1998**, *68* (5), 747−763.

DOI: 10.1021/acs.macromol.8b02189
Macromolecules 2019, 52, 2120−2130